



RESEARCH ARTICLE

Toxicological Assessment of Melamine-Functionalized Graphene Oxide and Carbon Nanotubes Using Zebrafish Models

¹Research Laboratory Application and Research Center (ALUM), Igdir University, Igdir, Türkiye | ²Department of Pharmacy Services, Tuzluca Vocational School, Igdir University, Igdir, Türkiye | ³Department of Pathology, Veterinary Faculty, Ataturk University, Erzurum, Türkiye | ⁴Department of Pathology, Veterinary Faculty, Kyrgyzstan-Türkiye Manas University, Bishkek, Kyrgyzstan | ⁵Igdir University, Department of Organic Agriculture Management, Faculty of Applied Sciences, Igdir, Türkiye | ⁶İzmir Biomedicine and Genome Center (IBG), Dokuz Eylul University Health Campus, Izmir, Türkiye | ⁷Department of Molecular Biology and Genetics, Izmir Institute of Technology, Izmir, Türkiye | ⁸Department of Seafood Processing Technology, Faculty of Fisheries, Ataturk University, Erzurum, Türkiye | ⁹Department of Aquaculture, Faculty of Fisheries, Ataturk University, Erzurum, Türkiye | ¹⁰Department of Biomedical Engineering, Faculty of Engineering, Necmettin Erbakan University, Konya, Türkiye | ¹¹Science Technology Research and Application Center (BITAM), Necmettin Erbakan University, Konya, Türkiye

 $\textbf{Correspondence:} \ Gunes \ Ozhan \ (gunesozhan@iyte.edu.tr) \ | \ Gonca \ Alak \ (galak@atauni.edu.tr) \ | \ Muhammed \ Atamanalp \ (mataman@atauni.edu.tr) \ | \ Nurettin \ Menges \ (nurettin.menges@erbakan.edu.tr)$

Received: 22 August 2025 | Revised: 16 September 2025 | Accepted: 23 September 2025

Funding: This work was supported by the Izmir Institute of Technology Scientific Research Projects under the program of ADEP (Project no: 2024IYTE-2-0012).

Keywords: carbon nanotubes | developmental toxicity | graphene oxide | melamine functionalization | nanoparticle | sensorimotor behavior | surface modification | zebrafish embryos

ABSTRACT

Graphene oxide (GO) and carbon nanotube (CNT)-based nanomaterials have attracted significant interest in various industrial and biomedical applications due to their unique physicochemical properties; however, concerns about their potential toxicity, especially when modified with additives like melamine (M), remain largely unresolved. This study investigates the toxicological effects and underlying mechanisms of graphene oxide-melamine (GO-M) and carbon nanotube-melamine (CNT-M) nanoparticles in zebrafish (*Danio rerio*) embryos and larvae. To this end, developmental toxicity, phenotypic and behavioral changes, as well as histopathological and immunofluorescence alterations, were evaluated following acute exposure to GO-M and CNT-M nanoparticles at concentrations of 5, 10, and 20 mg/L. Results showed that both nanoparticles delayed larval hatching, particularly at higher concentrations (10 and 20 mg/L). Malformations were observed at 20 mg/L in the GO-M group and at 10 and 20 mg/L in the CNT-M group. Additionally, significant changes in larval length and eye area were observed at all concentrations for both nanoparticles. Behavioral assessments revealed that CNT-M exposure at 10 and 20 mg/L significantly impaired head sensorimotor reflexes, while all concentrations affected tail reflexes. In contrast, GO-M exposure did not significantly alter sensorimotor responses. These findings suggest differential toxic mechanisms and neurobehavioral effects of GO-M and CNT-M nanoparticles during early zebrafish development.

© 2025 John Wiley & Sons Ltd.

1 | Introduction

Melamine is a nitrogen-rich compound widely used in both industrial and domestic applications, including paints, coatings, foam seating, bedding, automobile brake pipes, paper products, shelving, and mechanical, electrical, and plumbing concretes. It is also found in automobile inks, fabric softeners, or laundry detergents. Additionally, melamine is used as a coating for concrete surfaces, in automobile-formaldehyde resins, and in agricultural products such as seed coatings, plant protection agents, fertilizers, and algicides (An et al. 2013; Taşci et al. 2022; Lütjens et al. 2023; Day et al. 2024; Wang et al. 2025). Due to its extensive and diverse use, melamine enters various environmental compartments, particularly aquatic ecosystems, where it can pose a risk to nontarget organisms. Despite this, melamine's environmental fate and its potentially harmful effects on aquatic organisms, regarding their extent, severity, mechanisms, and ecological implications, have not been comprehensively investigated in aquatic environments. Nanomaterials such as GO and CNTs have attracted significant attention for their large surface area, high electrical conductivity, and chemical reactivity, making them useful in electronics, biomedicine, and environmental remediation (Ghulam et al. 2022; Yahyazadeh et al. 2024). Functionalization with compounds such as melamine can enhance their catalytic activity and electron transfer capabilities. However, these surface modifications may also alter their interactions with biological systems, potentially leading to unexpected toxic effects (Mohammadi et al. 2020; Ghulam et al. 2022).

Understanding how these functionalized nanomaterials interact with aquatic organisms is critical for assessing their safety. Environmental pollutants are known to disrupt various cellular processes and biomolecules, forming complex toxicity networks (Huang 2023). Bioassays and biomarkerbased approaches are therefore essential tools in ecotoxicological assessments (Molino et al. 2025). Among the molecular biomarkers, Nop10 (nucleolar protein 10) plays a vital role in the assembly of H/ACA small nucleolar ribonucleoproteins (snoRNPs), which are involved in maintaining telomerase function and genomic stability. Telomerase activity, in turn, protects telomere length; its dysfunction can trigger cellular senescence or apoptosis (Dou et al. 2024). Oxidative stress is a common pathway by which many pollutants exert their toxic effects. Reactive oxygen species (ROS) such as hydroxyl radicals can cause DNA strand breaks, base modifications, and DNA-protein cross-linking. Among the oxidative DNA damage markers, 8-hydroxy-2'-deoxyguanosine (8-OHdG) is widely studied as a reliable indicator of genotoxicity and oxidative stress (Alak, Ucar, Yeltekin, Çomaklı, et al. 2018; Alak, Ucar, Yeltekin, Parlak, et al. 2018; Alak, Yeltekin, Özgeriş, et al. 2019; Alak, Yeltekin, Uçar, et al. 2019; Alak et al. 2020; Uçar et al. 2020; Atamanalp et al. 2021).

Zebrafish (*Danio rerio*) has emerged as a powerful model organism in environmental toxicology due to its small size, high fecundity, transparent embryos, and ease of maintenance. Zebrafish embryos are particularly useful for assessing developmental toxicity and sublethal effects of pollutants. The Fish Embryo Acute Toxicity (FET) test using zebrafish is recognized

by international regulatory agencies and widely employed in environmental risk assessments (Alak et al. 2025; Yıldırım et al. 2025; Molino et al. 2025).

In this study, we aimed to investigate the potential toxicity mechanisms of GO and CNT nanoparticles functionalized with melamine (GO-M and CNT-M) in zebrafish embryos and larvae. Melamine was selected as a surface modifier to enhance the nanoparticles' functional properties. We evaluated a comprehensive set of effect-based parameters, including developmental, morphological, behavioral, histopathological, and immunohistochemical endpoints. Our goal was to elucidate the differential toxicity profiles of GO-M and CNT-M nanoparticles and contribute to a better understanding of their environmental safety.

2 | Materials and Methods

Thionyl chloride $(SOCl_2)$, graphite, sodium nitrate $(NaNO_3)$, potassium permanganate $(KMnO_4)$, hydrogen peroxide (H_2O_2) , hydrochloric acid (HCl), sulfuric acid (H_2SO_4) , anhydrous dimethylformamide (DMF), anhydrous tetrahydrofuran (THF), anhydrous diethyl ether, and melamine (M) were all purchased from Sigma–Aldrich (St Louis, MO, USA). Functionalized multi-walled carbon nanotubes (MWCNTs) containing surface carboxylic acid (-COOH), with a purity > 96% and an outer diameter of $8-18\,\mathrm{nm}$, were obtained from Nanografi (Ankara, Türkiye).

2.1 | Synthesis of CNT-M and GO-M Nanoparticles

2.1.1 | Synthesis of CNT-M Nanoparticles

To synthesize melamine-functionalized CNT-M, a two-step procedure was followed. First, 100 mg of commercially available carboxyl-functionalized multi-walled carbon nanotubes (MWCNTs-COOH) were added to a 100 mL glass flask along with 10 mL of SOCl2 and 1 mL of anhydrous DMF. The mixture was stirred at 70°C and 500 rpm for 24h on alternate days to convert the carboxyl groups to acyl chloride groups (CNT-Cl). After the reaction, the resulting product was filtered using a Gooch crucible (No. 4) and thoroughly washed with anhydrous diethyl ether, anhydrous THF, and anhydrous DMF to remove any residual reagents. The product was then dried in an oven at approximately 60°C. In the second step, 100 mg of CNT-Cl and 100 mg of melamine were added to a 100 mL round-bottom flask containing 3 mL of anhydrous DMF. The reaction mixture was stirred sequentially at 25°C for 1 h, 50°C for 1 h, and finally at 153°C for 22 h. Following the reaction, the solid product (CNT-M) was filtered using a Gooch crucible (No. 4), washed with anhydrous DMF, and dried in a low-temperature oven. The final CNT-M product was characterized using Fourier-transform infrared spectroscopy (FT-IR) with a PerkinElmer Spectrum Two spectrometer (Perkin Elmer, MA, USA), X-ray diffraction (XRD) using an Empyrean X-ray diffractometer (Malvern Panalytical, Spectris, London, UK), field emission scanning electron microscopy (FE-SEM) using a Hitachi Regulus 8230 (Hitachi

High-Tech, Tokyo, Japan), and transmission electron microscopy (TEM) using Hitachi HT7800 TEM (Hitachi High-Tech, Tokyo, Japan) (Figure 1).

2.1.2 | Synthesis of GO-M Nanoparticles

The synthesis of melamine-functionalized graphene oxide (GO-M) nanoparticles was carried out in three main steps: GO synthesis, acyl chloride functionalization (GO-Cl), and subsequent melamine modification. First, GO was synthesized using the modified Hummer method as described previously (Bulut et al. 2016). Briefly, 5g of graphite, 2.5g of NaNO₃, and 115 mL of concentrated H_2SO_4 (98%) were added to a round-bottom flask and stirred at 600 rpm for 30 min while kept in an ice bath to maintain the temperature below 20°C. After this initial step, 15 g of potassium permanganate (KMnO₄) was gradually added under continuous stirring, and the reaction was allowed to proceed for an additional hour. The mixture was then heated to 45°C, and 230 mL of deionized water was slowly added, followed by stirring for another 15 min. Afterwards, 230 mL of pure water was added, and the mixture was heated again at 45°C for 30 min. Finally, 600 mL of deionized water and 150 mL of 9% H₂O₂ were added, and the suspension was stirred for 1h. The resulting GO was filtered, thoroughly washed with deionized water and 5% HCl, and then dried in a low-temperature oven (Figure 2) (Bulut et al. 2016; Celebi and Söğüt 2022).

In the second step, $50\,\mathrm{mg}$ of the synthesized GO was reacted with $10\,\mathrm{mL}$ of SOCl_2 and $1\,\mathrm{mL}$ of anhydrous DMF in a $50\,\mathrm{mL}$ glass flask. The mixture was stirred at $70\,^\circ\mathrm{C}$ and $500\,\mathrm{rpm}$ on alternate days to convert oxygen-containing groups on the GO surface to acyl chlorides (GO-Cl). The solid product was collected by filtration using a Gooch crucible (No. 4), washed sequentially with anhydrous diethyl ether, THF, and DMF, and then dried at low temperature for further use (Figure 3) (Köktürk et al. 2022; Amudi et al. 2023).

In the final step, 100 mg of GO-Cl, 100 mg of melamine were added to 3 mL of anhydrous DMF in a 100 mL round-bottom flask. The mixture was stirred sequentially at 25°C for 1 h, 50°C for 1 h, and finally at 153°C for 22 h to facilitate the functionalization reaction. After completion, the reaction mixture was filtered using a Gooch crucible (No. 4), and the solid product was washed with anhydrous DMF. The resulting GO-M nanoparticles were dried in a low-temperature oven and characterized

FIGURE 1 | Schematic illustration of the surface functionalization of multi-walled carbon nanotubes (MWCNTs) with melamine.

FIGURE 2 | Schematic illustration of the synthesis process of graphene oxide (GO) using the modified Hummers method.

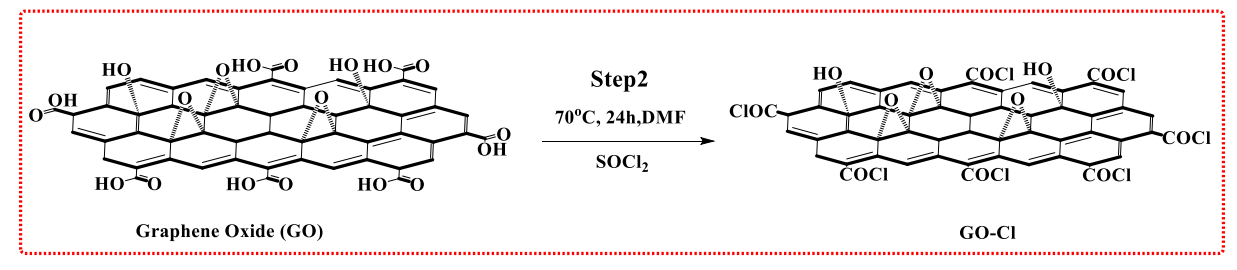


FIGURE 3 | Schematic illustration of the synthesis of acyl chloride-functionalized graphene oxide (GO-Cl) from GO using SOCl, and DMF.

FIGURE 4 | Schematic illustration of the synthesis of melamine-functionalized graphene oxide (GO-M) through from GO-Cl via melamine coupling.

using FT-IR, FE-SEM, TEM, and XRD (Figure 4) (Köktürk et al. 2022; Amudi et al. 2023).

28°C for the duration of the experiment.

concentration. All groups were maintained in an incubator at

2.2 | In Vivo Toxicity Assessment

2.2.1 | Zebrafish Care and Embryo Production

Adult zebrafish (wild-type AB line) were obtained from the Vivarium-Zebrafish Facility at the Izmir Biomedicine and Genome Center (IBG). Fish were maintained under standardized laboratory conditions at a water temperature of 28°C with a 14:10-h light-dark photoperiod, following established protocols (Westerfield 2000). Water quality parameters were routinely monitored, with pH maintained at 7.0-7.2 and dissolved oxygen levels above 6.0 mg/L during both the rearing and exposure periods. They were fed twice daily with a combination of flake feed and Artemia. To obtain embryos for experimentation, male and female zebrafish were housed in separate breeding tanks. Spawning was induced overnight, and fertilized eggs were collected the following morning. Collected embryos were transferred to Petri dishes containing E3 embryo medium (0.17 mM KCl, 0.33 mM MgSO₄, 5 mM NaCl, and 0.33 mM CaCl₂). As the study involved zebrafish embryos and larvae under 5 days postfertilization (dpf), ethical approval was not required in accordance with Directive 86/609/EEC and EU Directive 2010/63/ EU.

2.2.2 | Exposure of Embryos and Larvae to GO-Melamine (GO-M) and CNT-Melamine (CNT-M)

The toxic effects of GO-M and CNT-M nanoparticles on zebrafish embryos and larvae were evaluated based on previously reported dose ranges (H. C. Chen et al. 2024; Yiğit et al. 2024; SinghDeo et al. 2025). Exposure experiments were initiated at 4h postfertilization (hpf) and continued until 96 hpf. Stock solutions of GO-M and CNT-M nanoparticles were prepared in purified water at a concentration of 100 mg/L. Working solutions at final concentrations of 5, 10, and 20 mg/L were freshly prepared each day by diluting the stock in E3 embryo medium. To minimize agglomeration and ensure homogeneity, all nanoparticle solutions were sonicated for 10 min at 50/60 kHz using a Huber Diagenode Mini Chiller (Germany) prior to use. The control group received E3 medium without nanoparticles. Each treatment group consisted of 30 embryos, with three replicates per

2.2.3 | Developmental Toxicity Evaluation

Developmental toxicity in zebrafish embryos and larvae was evaluated based on a previously described method with slight modifications (Alak et al. 2025). Parameters evaluated included mortality (24–96 hpf), morphological abnormalities (24–96 hpf), and chorion hatching rate (48–96 hpf) following exposure to GO-M and CNT-M nanoparticles. Embryos and larvae were examined and imaged using an Olympus SZX50 stereomicroscope equipped with an SC16 digital camera (Olympus, Tokyo, Japan).

2.2.4 | Phenotypic Evaluation of Zebrafish Larvae Body Length and Eye Size

To assess the phenotypic effects of GO-M and CNT-M nanoparticles, zebrafish larvae were evaluated at 96 hpf. Ten larvae from each experimental group were imaged using a stereomicroscope (Olympus, Tokyo, Japan). Morphometric measurements, including body length (mm) and eye surface area (mm²), were performed using ImageJ software (Bridi et al. 2017; Wang et al. 2024).

2.2.5 | Behavioral Evaluation With Sensory Motor Reflex

To assess the potential neurobehavioral effects of GO-M and CNT-M nanoparticles, sensory-motor reflex responses were evaluated at 96 hpf. The heads and tails of larvae (n=5 per group, in triplicate) were gently stimulated using a micropipette. Each region was touched 10 times at 30-s intervals. A positive response was defined as a sudden escape or swimming reflex following stimulation (Cunha et al. 2018; Rodrigues et al. 2020; Yiğit et al. 2024).

2.2.6 | Histopathological Evaluation and Immunofluorescence Analysis of Zebrafish Larvae

2.2.6.1 | **Histopathological Examination.** Following experimental exposure, zebrafish larvae were fixed in 10%

neutral-buffered formalin for 48 h. After standard tissue processing, samples were embedded in paraffin, and $4\mu m$ -thick sections were obtained. The sections were stained with hematoxylin–eosin (H&E) and examined under an Olympus BX 51 light microscope (Olympus, Japan). Histopathological alterations were scored semi-quantitatively as none (–), mild (+), moderate (++), or severe (+++) based on the extent and severity of observed tissue changes.

2.2.6.2 | Double Immunofluorescence Examination. For double immunofluorescence analysis, tissue sections were mounted on adhesive slides (poly-L-lysine-coated), deparaffinized, and dehydrated through graded alcohols. Endogenous peroxidase activity was blocked by incubating the sections in 3% H₂O₂ for 10 min. Antigen retrieval was performed by boiling the tissues in 1% citrate buffer solution (pH 6.1, 100X) followed by cooling to room temperature. To minimize nonspecific background staining, sections were incubated with a protein blocking solution for 5 min. The first primary antibody, anti-8-OHdG (Cat No: sc393871, dilution 1:100, Santa Cruz Biotechnology, TX, USA), was applied and incubated according to the manufacturer's instructions. After washing, the corresponding secondary antibody conjugated with FITC (Cat No: ab6785, dilution 1:1000, Abcam, Cambridge, UK) was applied and incubated for 45 min in the dark. Subsequently, the second primary antibody, anti-NOP10 (Cat No: ab134902, dilution 1:100, Abcam, Cambridge, UK), was applied and incubated according to the manufacturer's instructions. Afterward, a Texas Red-conjugated secondary antibody (Cat No: ab6719, dilution 1:1000, Abcam, Cambridge, UK) was added and incubated for 45 min in the dark. Nuclear counterstaining was performed using DAPI-containing mounting medium (Cat No: D1306, dilution 1:200, MA, USA), which was applied to the sections and incubated for 5 min in the dark. Finally, coverslips were placed on the slides, and the stained sections were examined under a fluorescence microscope (Carl Zeiss AG, Jena, Germany).

2.2.7 | Data Analysis

Developmental toxicity, behavioral, and histopathological data were analyzed using GraphPad Prism 8 software. Results are expressed as mean \pm standard deviation (mean \pm SD), with statistical significance considered at the following levels: *p<0.05, **p<0.01, ***p<0.001, ****p<0.0001, and not significant (ns) for p>0.05. Developmental toxicity endpoints, including survival rate, malformations, body length, eye size, and behavioral responses, were evaluated using one-way analysis of variance (ANOVA). Tukey's multiple comparison test was applied for survival rate, malformations, body length, and eye size, while Dunnett's test was used for behavioral data. The Shapiro–Wilk test was used to assess the normality of behavioral datasets. Chorion hatching success was analyzed via two-way ANOVA followed by Tukey's post hoc test.

For histopathological evaluations, the Duncan test was used to compare differences between groups. Group interactions were assessed using the nonparametric Kruskal–Wallis test, and pairwise comparisons were made using the Mann–Whitney U test. Quantitative analysis of immunofluorescence staining was conducted using the ZEISS Zen Imaging Software (Carl Zeiss

AG, Jena, Germany). Five random regions were selected from each image to evaluate fluorescence intensity. The percentage of positively stained area was reported as mean ±SD. Comparisons between groups and healthy controls were made using one-way ANOVA followed by Tukey's multiple comparison test. A *p*-value of less than 0.05 was considered statistically significant.

3 | Results and Discussion

3.1 | Functional Group Identification via FT-IR Analysis

FT-IR spectroscopy was performed using the KBr pellet method with a PerkinElmer Spectrum Two spectrometer, covering the 600-4000 cm⁻¹ range with a 4 cm⁻¹ resolution, to confirm the functionalization of GO and MWCNTs with melamine. For CNT-M, a characteristic vibration band was observed at 3128 cm⁻¹, corresponding to the N-H stretching of primary amine groups (-NH₂) from melamine (Figure 5). The 1673 cm^{−1} band was attributed to C=O stretching from amide groups (-HNC=O), indicating successful amide bond formation. Additionally, the 1551 cm⁻¹ band was assigned to C=N stretching vibrations of the imine group within the melamine ring. In the GO-M spectrum, similar functional groups were confirmed (Figure 5). The 3117 cm⁻¹ band indicated N-H stretching (-NH₂), and the 1676 cm⁻¹ peak corresponded to C=O stretching in the amide group. The C=N group was represented by a vibration band at $1507\,\mathrm{cm^{-1}}$, while a notable additional peak at 1096 cm⁻¹ was attributed to C-N stretching, confirming the presence of melamine on the GO surface (Zhang et al. 2011; Yuan et al. 2015; Feng et al. 2018; Amudi et al. 2023). In conclusion, FT-IR results confirmed the successful covalent attachment of melamine to both GO and CNT surfaces through amide bond formation and the presence of characteristic imine and amine groups.

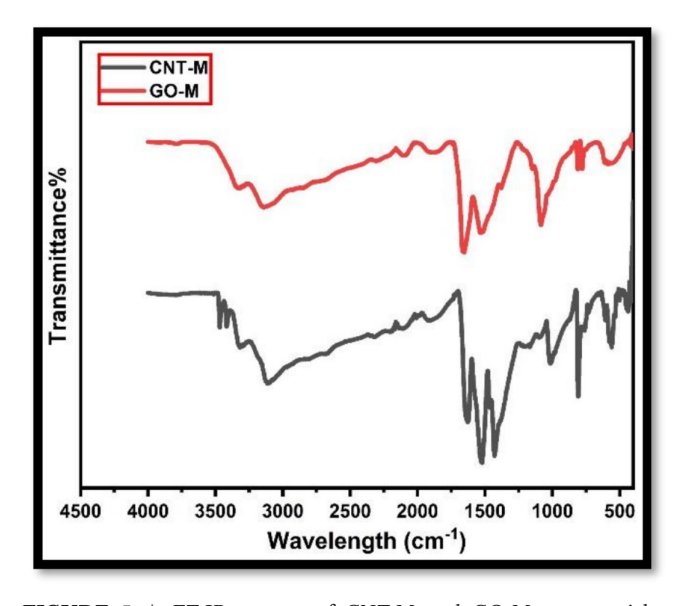


FIGURE 5 | FT-IR spectra of CNT-M and GO-M nanoparticles, showing characteristic functional group vibrations confirming successful melamine functionalization. Key peaks corresponding to $-NH_2$, C=O (amide), C=N (imine), and C-N groups are observed.

3.2 | XRD Analysis Reveals Structural Changes and Crystallite Sizes of CNT-M and GO-M Nanoparticles

XRD analysis was performed to investigate the structural properties, crystallinity, and phase identification of GO-M and CNT-M. The XRD measurements were conducted using a Panalytical Empyrean diffractometer with Cu K α radiation (λ =1.540598 nm), operating at 45 kV and 40 mA. The scanning was performed from 5° to 90° (2 θ) at a rate of 2°/min for 20 min.

For CNT-M, a prominent diffraction peak was observed at $2\theta = 25.09^{\circ}$, characteristic of the (002) plane of MWCNTs, consistent with earlier studies (Figure 6) (Zhu et al. 2008; Salam and Burk 2017). Additional broad peaks between $2\theta = 10^{\circ}$ and 30° indicate the presence of melamine-functionalized structures. Although the modification did not significantly alter the position of the characteristic CNT peak, an increase in intensity and peak density suggests successful surface modification. This observation aligns with previous findings indicating that melamine's π - π interactions, hydrogen bonding, and electrostatic interactions enhance surface interactions without disrupting the CNT

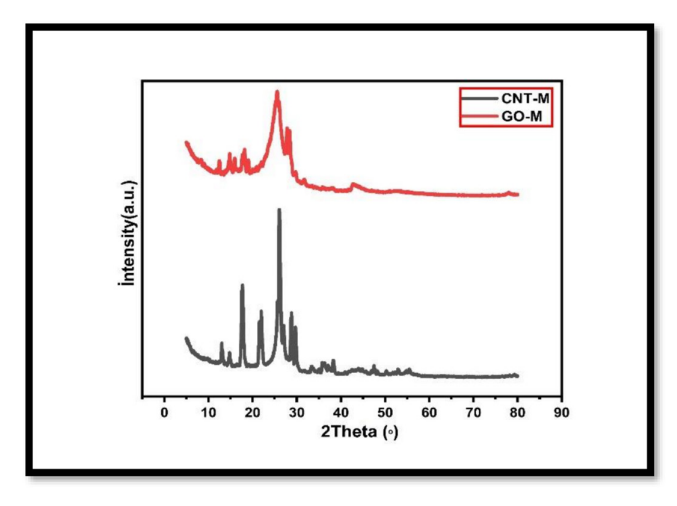


FIGURE 6 | XRD diffraction patterns of CNT-M and GO-M nanoparticles, indicating characteristic crystalline peaks and structural changes resulting from surface modification.

crystalline core (Irani et al. 2017). The XRD pattern of GO-M revealed a peak at $2\theta = 12.33^{\circ}$, which is characteristic of GO, corresponding to the (001) plane (Figure 6). A distinct and intense peak at $2\theta = 28^{\circ}$ was attributed to structural modifications due to melamine intercalation, suggesting a successful interaction between GO layers and melamine molecules (Y. Chen et al. 2011; Yuan et al. 2015). This intercalation likely alters the interlayer spacing and modifies surface functionalities.

Crystallite size (D) was calculated in nanometers using the Debye–Scherrer equation (Equation 1):

$$D = 0.9\lambda/(\beta \cos\theta) \tag{1}$$

where k is the shape factor (0.9), λ is the X-ray wavelength (0.15406nm), β is the full width at half maximum (FWHM) of the diffraction peak, and θ is the Bragg angle. Based on this calculation, the average crystallite sizes of GO-M and CNT-M were determined to be 43.02 and 90.20nm, respectively (Manzoor et al. 2024). In conclusion, XRD analysis confirmed the crystalline nature of CNT-M and GO-M, with distinct diffraction patterns and crystallite sizes supporting the successful functionalization of both nanomaterials with melamine. The observed structural changes, particularly in GO-M, suggest effective intercalation and surface interaction of melamine, likely driven by strong π - π and electrostatic forces (León et al. 2011; Liang et al. 2012; Leon et al. 2014).

3.3 | Surface Morphology and Elemental Composition of CNT-M and GO-M Nanoparticles

The morphological characteristics and surface modifications of CNT-M and GO-M were analyzed using FE-SEM. Figure 7 presents the FE-SEM micrographs of CNT-M and GO-M. Consistent with previous studies, unmodified MWCNTs exhibit smooth, translucent, and tubular surfaces (Veisi et al. 2019). Following melamine functionalization, the CNT surfaces appeared rougher and more curved, accompanied by partial aggregation (Peng et al. 2018; H. Shayesteh et al. 2023). In the GO-M samples, typical sheet-like layered structures were clearly observed (Sun et al. 2019). Upon melamine modification, noticeable surface wrinkling and edge curling were frequently detected. These morphological alterations suggest

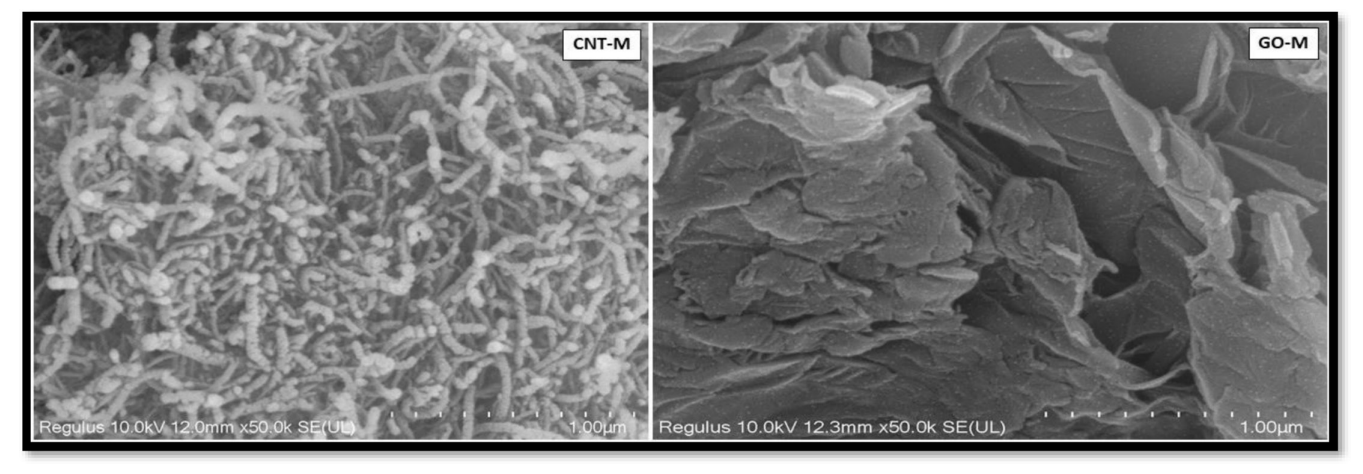


FIGURE 7 | FE-SEM images of CNT-M and GO-M nanomaterials, illustrating their surface morphology and structural features.

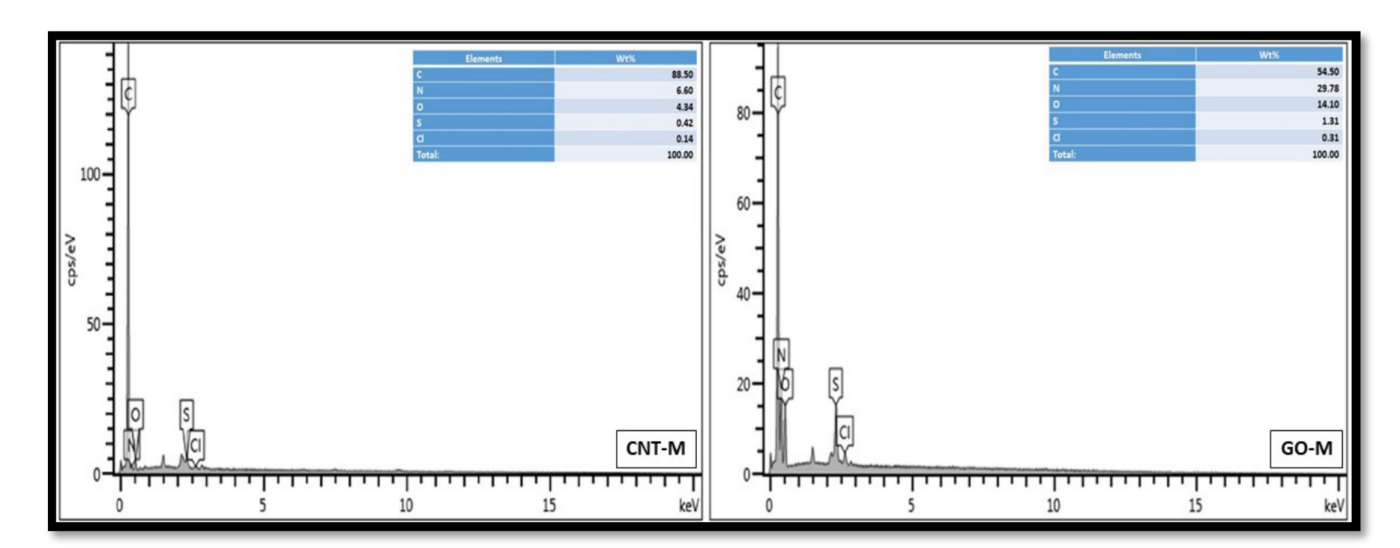


FIGURE 8 | EDX spectra of CNT-M and GO-M nanoparticles showing elemental composition and successful incorporation of nitrogen after melamine functionalization.

that melamine intercalation disrupts the planar structure of GO, leading to increased interlayer spacing and the formation of localized tears.

The elemental composition of CNT-M and GO-M was determined using energy dispersive X-ray spectroscopy (EDX) coupled with FE-SEM. As shown in Figure 8, the EDX spectrum of CNT-M revealed signals for carbon (C), oxygen (O), and nitrogen (N), with atomic percentages of 88.52%, 4.34%, and 6.6%, respectively. Trace signals from other elements were attributed to residual impurities from the washing process (Mao et al. 2020; H. Shayesteh et al. 2023; Algethami et al. 2024). In the case of GO-M, atomic percentages were determined as 54.50% C, 29.78% O, and 14.10% N (Sun et al. 2019; Sen et al. 2021). The higher nitrogen content in GO-M suggests a more effective binding of melamine rings, likely due to the abundant oxygen-containing functional groups on the GO surface. In contrast, commercially available MWCNTs typically contain only 3%-5% COOH groups, limiting melamine attachment efficiency. In summary, FE-SEM and EDX analyses demonstrated that melamine functionalization alters the surface morphology of both CNT and GO nanostructures. The findings also indicate a more efficient melamine incorporation in GO-M, attributed to the greater surface reactivity of GO compared to CNTs.

3.4 | TEM Imaging Reveals Morphological Integrity and Size Distribution of CNT-M and GO-M Nanoparticles

TEM was performed using a Hitachi HT7800 model TEM operated at 100 kV with a magnification of ×40,000 to evaluate the morphological integrity and size distribution of CNT-M and GO-M nanostructures. As shown in Figure 9, the TEM images of CNT-M confirm the preservation of the characteristic multilayered cylindrical structure of MWCNTs after melamine functionalization (Figure 9, top left). No apparent deformation or collapse of the tubular structure was observed. Diameter analysis performed on 10 individual CNT-M particles revealed

an average diameter of $10.73 \pm 2.26 \,\mathrm{nm}$ (range: $5.70 - 12.99 \,\mathrm{nm}$), which remains consistent with the nominal outer diameter (8-18 nm) provided by the commercial supplier (Figure 9, bottom left). This suggests that the surface modification with melamine did not significantly alter the tubular morphology of CNTs (Banerjee and Wong 2002; Deng et al. 2015; Gupta et al. 2019). In contrast, the TEM images of GO-M exhibit both dark and light regions, indicating heterogeneity in electron density (Figure 9, top right). These features likely correspond to the presence of oxygen-rich functional groups on the GO layers and the distribution of melamine molecules across the surface. Wrinkles and folds observed in the GO-M sheets may reflect interlayer expansion or partial exfoliation induced by melamine intercalation. Particle size analysis of 10 GO-M structures yielded an average diameter of 19.51 ± 2.76 nm (range: 12.59-21.23 nm), which is consistent with previous reports for similarly functionalized graphene-based materials (Figure 9, bottom right) (Jebaranjitham et al. 2019; Köktürk et al. 2022; Borah et al. 2024). In conclusion, TEM analysis confirmed that melamine modification preserved the structural integrity of CNTs and induced slight morphological alterations in GO, consistent with successful functionalization.

3.5 | Effects of GO-M and CNT-M Nanoparticles on Zebrafish Survival and Hatching Rates

The developmental toxicity assessment revealed that zebrafish embryos and larvae exposed to GO-M at concentrations of 5 and $10\,\text{mg/L}$ and to CNT-M at $5\,\text{mg/L}$ maintained survival rates above 90% (Figure 10A). However, a statistically significant reduction in survival was observed in the GO-M $20\,\text{mg/L}$ group and in the CNT-M 10 and $20\,\text{mg/L}$ groups compared to the control. Additionally, a concentration-dependent delay in hatching was noted at 48, 72, and $96\,\text{h}$ postfertilization, particularly in the 10 and $20\,\text{mg/L}$ exposure groups for both nanoparticle types (Figure 10B). In contrast to our findings, previous studies involving melamine-containing polymeric microspheres ($1-5\,\mu\text{m}$, $0.1\,\text{mg/L}$) reported more pronounced developmental toxicity in $Daphnia\,magna$, including reduced

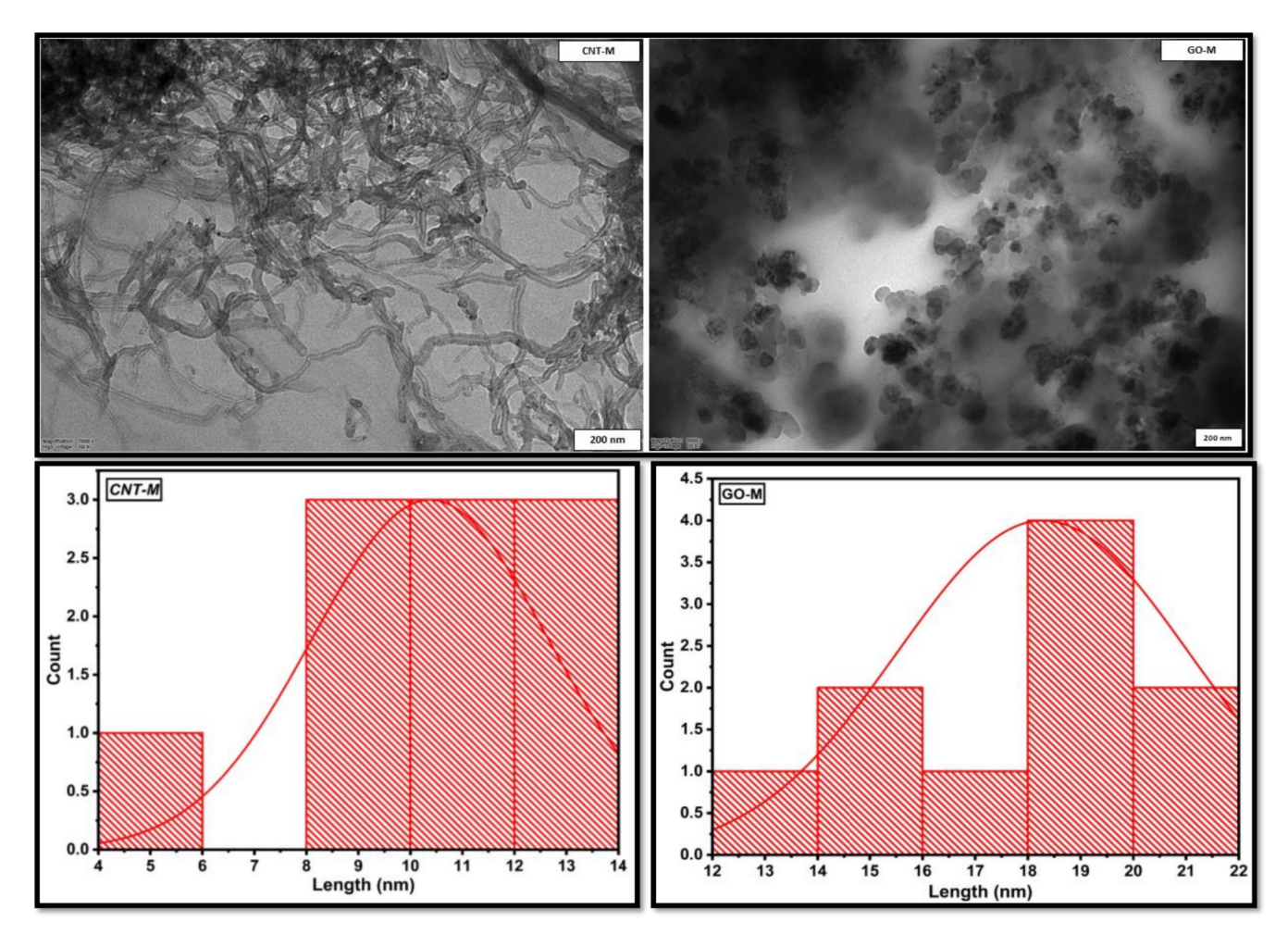


FIGURE 9 | TEM images and corresponding particle size distribution histograms of CNT-M and GO-M nanostructures. The images display the morphological characteristics of CNT-M and GO-M, while the histograms represent the measured particle diameters based on analysis of 10 individual particles for each sample.

growth and reproduction, increased mortality (up to 100%), and extinction of the F1 generation (Li et al. 2025). Similarly, prolonged exposure to polystyrene microspheres (5 μ m, 5 μ g/L, and 5 mg/L) led to significant reductions in offspring production across two generations. In conclusion, while lower concentrations of GO-M and CNT-M (\leq 10 mg/L) were relatively non-toxic to zebrafish embryos, higher concentrations (\geq 10 mg/L) induced developmental toxicity, evidenced by decreased survival and delayed hatching.

3.6 | Teratogenic Effects and Morphological Malformations Caused by GO-M and CNT-M Nanoparticles

Malformations including pericardial edema, spinal curvature, and tail deformities were observed in zebrafish larvae following 96 h of exposure to GO-M and CNT-M nanoparticles (Figure 11A). Compared with the control group, malformation rates were significantly higher in larvae exposed to 10 and $20\,\mathrm{mg/L}$ CNT-M and $20\,\mathrm{mg/L}$ GO-M (Figure 11B).

The reduced larval emergence rate at the highest concentration of GO-M ($20\,mg/L$) may be attributed to the adherence of GO

to the embryo surface, potentially inducing a hypoxic environment and restricting embryonic movement (Z. Chen et al. 2020). Supporting this, X. Chen et al. (2016) reported that GO particles can attach to the chorion via hydroxyl interactions and may infiltrate pore channels through passive diffusion. Another study has similarly demonstrated that GO exposure in zebrafish results in elevated embryonic mortality, cardiotoxicity, delayed cardiac cycles, apoptosis, reduced hemoglobinization, and abnormal hatching patterns (Bangeppagari et al. 2019).

Our findings confirm that GO-M at 20 mg/L induces notable deformities, particularly pericardial edema, tail abnormalities, and spinal curvature, which align with previous reports (X. Chen et al. 2016; Bangeppagari et al. 2019; Z. Chen et al. 2020; Köktürk et al. 2022). In addition, GO has been shown to interfere with embryonic development via increased ROS production, mitochondrial damage, genotoxicity, and metabolic disruptions (Bangeppagari et al. 2019).

A dose-dependent increase in mortality and malformation rates as well as a decrease in hatching were observed with CNT-M, particularly at 10 and $20\,\text{mg/L}$. These results are consistent with previous nanoparticle toxicity studies (Köktürk et al. 2022, 2023; Yiğit et al. 2024). While functionalized CNTs have previously

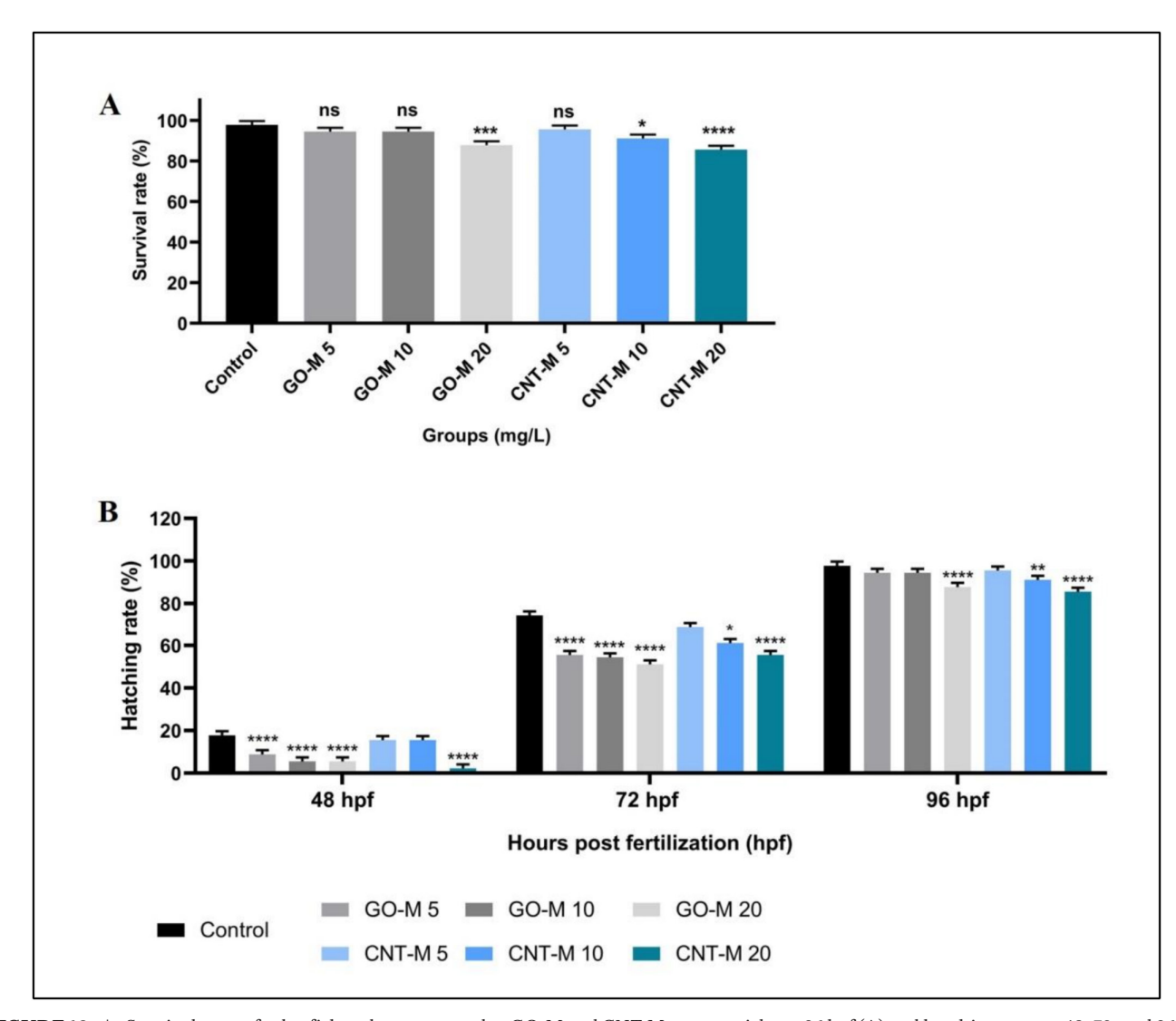


FIGURE 10 | Survival rates of zebrafish embryos exposed to GO-M and CNT-M nanoparticles at 96 hpf (A) and hatching rates at 48, 72, and 96 hpf (B). Data are presented as mean \pm SD. Statistical significance compared to the control group is indicated as follows: *p<0.05, **p<0.001, ****p<0.001; ns not significant (ns) for p>0.05.

been reported as nontoxic in zebrafish embryos and even shown to be excreted within 144h in *Gobiocypris rarus* fry (Zhao et al. 2024), our findings suggest that melamine-modified CNTs at higher doses exhibit significant developmental toxicity.

Zebrafish embryos are naturally protected by the chorion, which acts as a barrier to nanoparticle entry. In this study, low concentrations of GO-M (5 and $10\,\text{mg/L}$) and CNT-M (5 mg/L) did not induce significant malformations or mortality, suggesting a relatively safe profile at these levels. Moreover, despite the observed effects at $20\,\text{mg/L}$, GO-M appeared to be less teratogenic than CNT-M at the same concentration, indicating a potentially safer margin at higher doses. GO-M and CNT-M nanoparticles exhibited dose-dependent developmental toxicity in zebrafish embryos, with higher concentrations leading to increased malformations and reduced hatching rates. However, low concentrations ($\leq 10\,\text{mg/L}$ for GO-M and $5\,\text{mg/L}$ for CNT-M) showed minimal toxic effects, suggesting concentration-dependent safety thresholds.

In our study, exposure to GO-M and CNT-M nanoparticles resulted in subtle but measurable changes in zebrafish larval phenotypes, including body length and eye area. While the differences in body length were modest, statistically significant variations were observed in both body length and eye area across all treatment groups compared to the control (Figure 12A,B). For eye area, although the changes were not strictly concentration-dependent, a general trend of reduction with increasing nanoparticle concentration was evident. This pattern suggests that the toxicity of melamine-functionalized nanoparticles may not scale linearly with dose, but instead exerts a mild and progressive impact on early eye development. These findings suggest that even low to moderate concentrations of surface-functionalized nanoparticles may influence early developmental parameters. Consistent with our observations, Li et al. (2025) reported that D. magna juveniles exposed to melamine exhibited a dose-dependent increase in abnormal offspring and a significant reduction in body length.

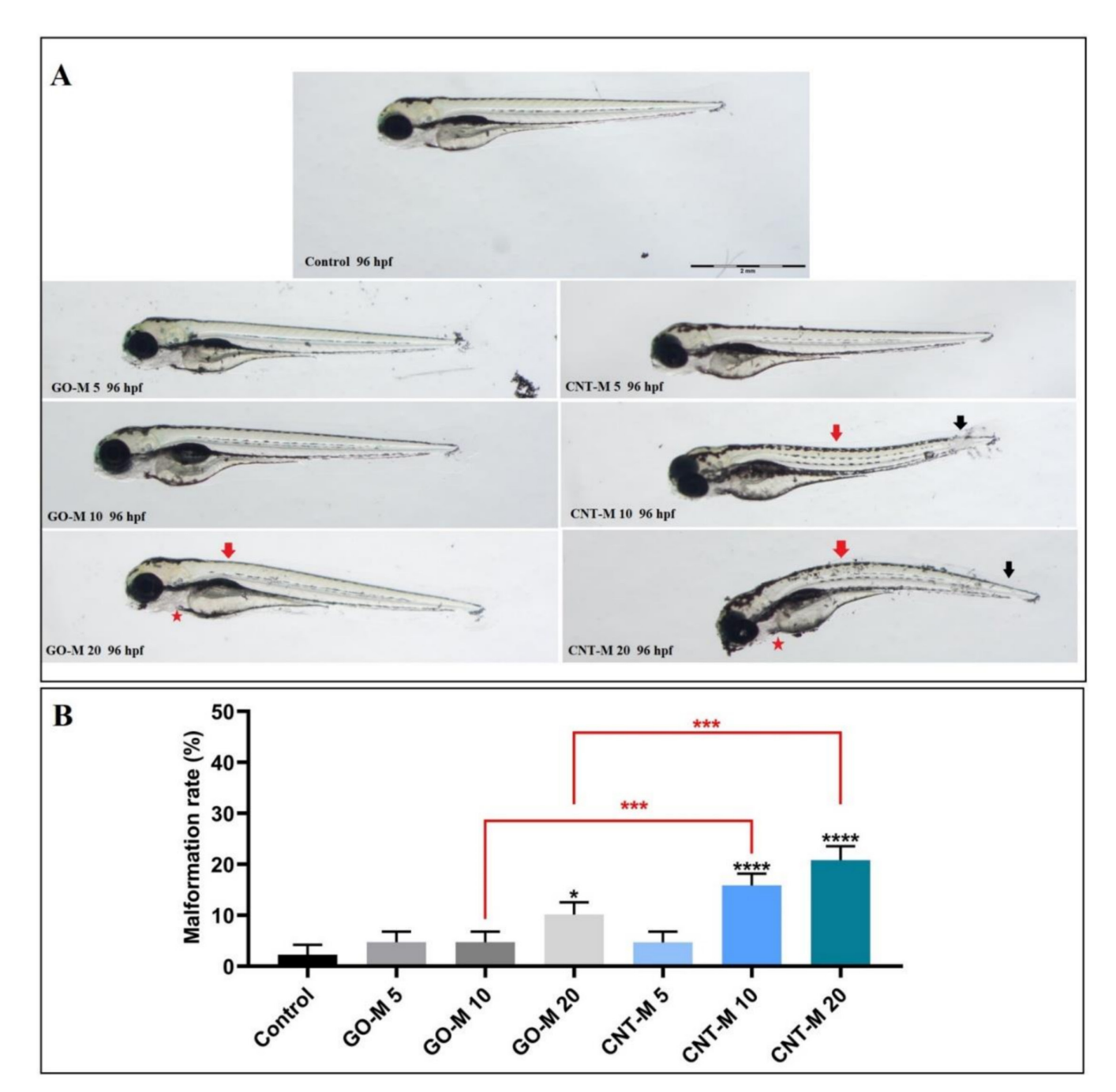


FIGURE 11 | (A) Representativbe microscope images showing morphological abnormalities in zebrafish larvae following 96-h exposure to GO-M and CNT-M nanoparticles. Observed malformations include pericardial edema (red arrow), spinal curvature (red arrow), and tail deformities (black arrow). Scale bar: 2 mm. (B) Quantification of malformation rates in zebrafish embryos and larvae exposed to increasing concentrations (5, 10, and $20 \, \text{mg/L}$) of GO-M and CNT-M. Data are presented as mean \pm SD Statistical significance: black asterisks indicate comparisons with the control group; red asterisks indicate comparisons between treatment groups (*p<0.05, ****p<0.001, ****p<0.0001).

3.7 | Neurobehavioral and Neurodevelopmental Effects of GO-M and CNT-M Nanoparticles

Head and tail sensorimotor reflexes were evaluated to investigate the potential neurotoxic effects of GO-M and CNT-M nanoparticles on zebrafish larvae. A significant reduction in head reflex responses was observed in larvae exposed to CNT-M at 10 and 20 mg/L (Figure 13A), while all CNT-M treatment groups showed a significant impairment in tail

reflex responses compared to the control group (Figure 13B). In contrast, exposure to GO-M nanoparticles at all tested concentrations did not lead to statistically significant changes in either head or tail reflexes (p > 0.05) (Figure 13A,B). Previous studies have suggested that melamine may adversely affect neuronal function by elevating ROS levels and enhancing autophagy in mesangial cells (Wang et al. 2015). In line with these findings, the observed sensorimotor impairments at higher CNT-M concentrations (10 and $20\,\text{mg/L}$) in our study

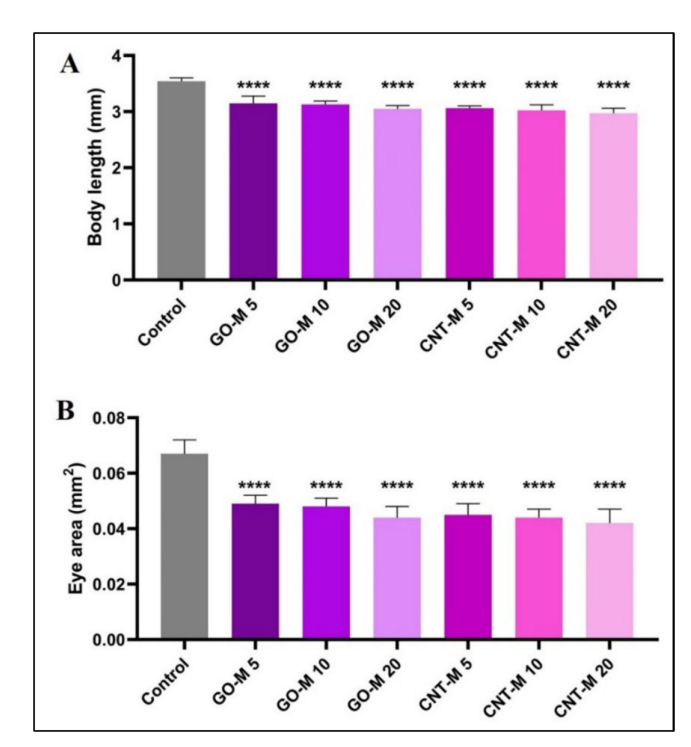


FIGURE 12 | Phenotypic assessment of zebrafish larvae exposed to different concentrations of GO-M and CNT-M nanoparticles. (A) Body length and (B) eye area measurements at 96 hpf. Data are presented as mean \pm SD ****p < 0.0001.

may be attributed to melamine-induced oxidative stress affecting neuronal circuits. Supporting this, An and Sun (2017) reported compelling evidence that neurons are particularly susceptible to melamine-induced damage.

When ingested, melamine may cause various health issues depending on the dose and duration of exposure. Although considered to have relatively low acute toxicity, melamine can hydrolyze to cyanuric acid at high concentrations, resulting in the formation of insoluble melamine cyanurate crystals, commonly referred to as kidney stones, and causing renal damage (Benedetto et al. 2011; Pei et al. 2011; An et al. 2013; Ahmed et al. 2021; Bashir et al. 2021, 2025; Taşci et al. 2022). In our study, the GO-M nanoparticle did not induce any significant changes in zebrafish behavior. Compared to previously reported behavioral toxicities of various solvents in zebrafish models, our phenomic analysis suggests that melamine exhibits relatively low neurobehavioral toxicity under systematic exposure or oral administration (H. C. Chen et al. 2024).

Due to their nanoscale dimensions, nanoparticles can readily penetrate the cells and tissues of aquatic organisms, particularly fish, where they may interfere with normal physiological processes (Kahru et al. 2008; Keller et al. 2010). In our study, CNT-M nanoparticles (average diameter: 10.378 nm) exhibited greater developmental toxicity than GO-M nanoparticles (average diameter: 18.284 nm), which may be attributed to the enhanced cellular penetration of smaller-sized CNT-M nanoparticles. Consistent with this, Z. Chen et al. (2020) reported that the developmental toxicity of GO in zebrafish larvae was closely related to its particle size. Small-sized nanoparticles also have

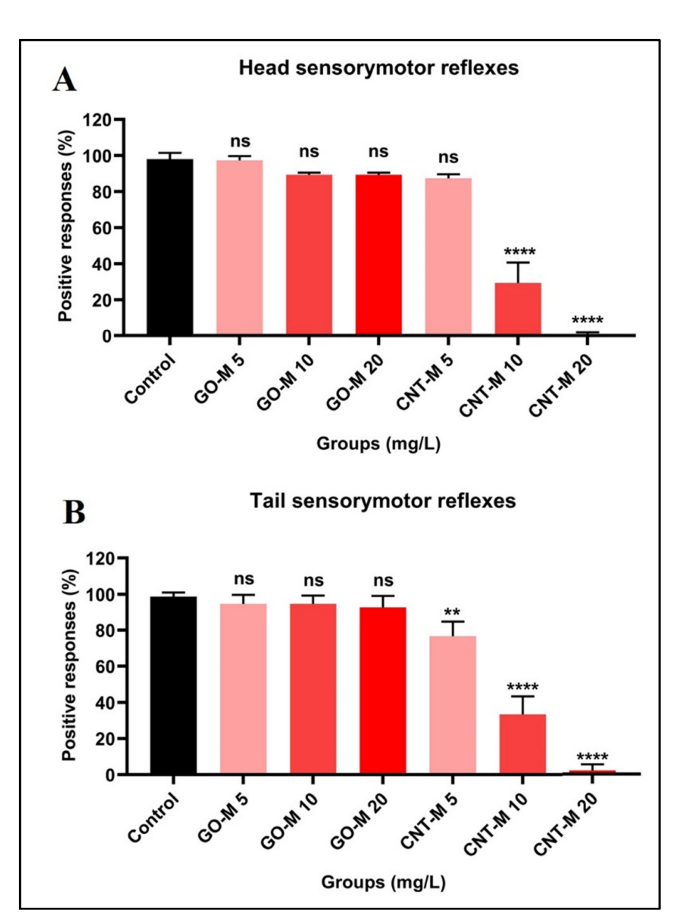


FIGURE 13 | Assessment of sensorimotor reflexes in zebrafish larvae exposed to different concentrations of GO-M and CNT-M nanoparticles at 96 hpf. (A) Head reflex response. (B) Tail reflex response. Asterisks indicate statistically significant differences compared to the control group. Data are presented as mean \pm SD (**p<0.01, ****p<0.0001, ns: not significant, p>0.05).

the potential to cross biological barriers such as the blood-brain barrier (BBB), leading to accumulation in the brain (Sharma et al. 2009). Once accumulated, they can induce oxidative stress, inflammation, and associated pathological changes, ultimately resulting in neurotoxicity (Karmakar et al. 2014). Moreover, the developing brain is particularly vulnerable to chemical insults, making embryos and larvae more susceptible to neurotoxic effects compared to adults (Bondy and Campbell 2005). Therefore, the potential neurodevelopmental toxicity of nanoparticles in zebrafish embryos and larvae warrants careful investigation (Fan et al. 2021).

The differing neurotoxic effects observed between CNT-M and GO-M can be explained by their distinct physicochemical characteristics, particularly morphology, size, and bioavailability. CNT-M exhibited a smaller average diameter (~10.7 nm) and a tubular geometry, which likely facilitated more efficient cellular uptake and penetration across the BBB. This enhanced bioavailability may account for the pronounced neurotoxic outcomes at higher concentrations, including reflex impairment, histopathological alterations, and elevated oxidative and nucleolar stress markers. In contrast, GO-M presented a larger average size (~19.5 nm) and a two-dimensional sheet-like morphology, which not only restricts

BBB penetration but also promotes surface adherence and aggregation. These features likely reduced its effective internal exposure, thereby minimizing neurotoxic manifestations. Our findings further highlight that while CNT-M possesses favorable dimensions for BBB passage, the relatively larger, sheet-like GO-M is less bioavailable to neural tissue under the tested conditions. The absence of measurable neurotoxic effects in the GO-M groups further underscores the critical role of nanoparticle morphology in determining biodistribution and organ-specific toxicity.

3.8 | Histopathological and Molecular Indicators of Neurotoxicity Induced by GO-M and CNT-M Nanoparticles

To evaluate the extent of damage in zebrafish brain tissue following exposure to varying concentrations of GO-M and CNT-M nanoparticles, histological examinations were performed using H&E staining (Figure 14). Brain tissues from the control group displayed normal histological architecture, with no evidence of

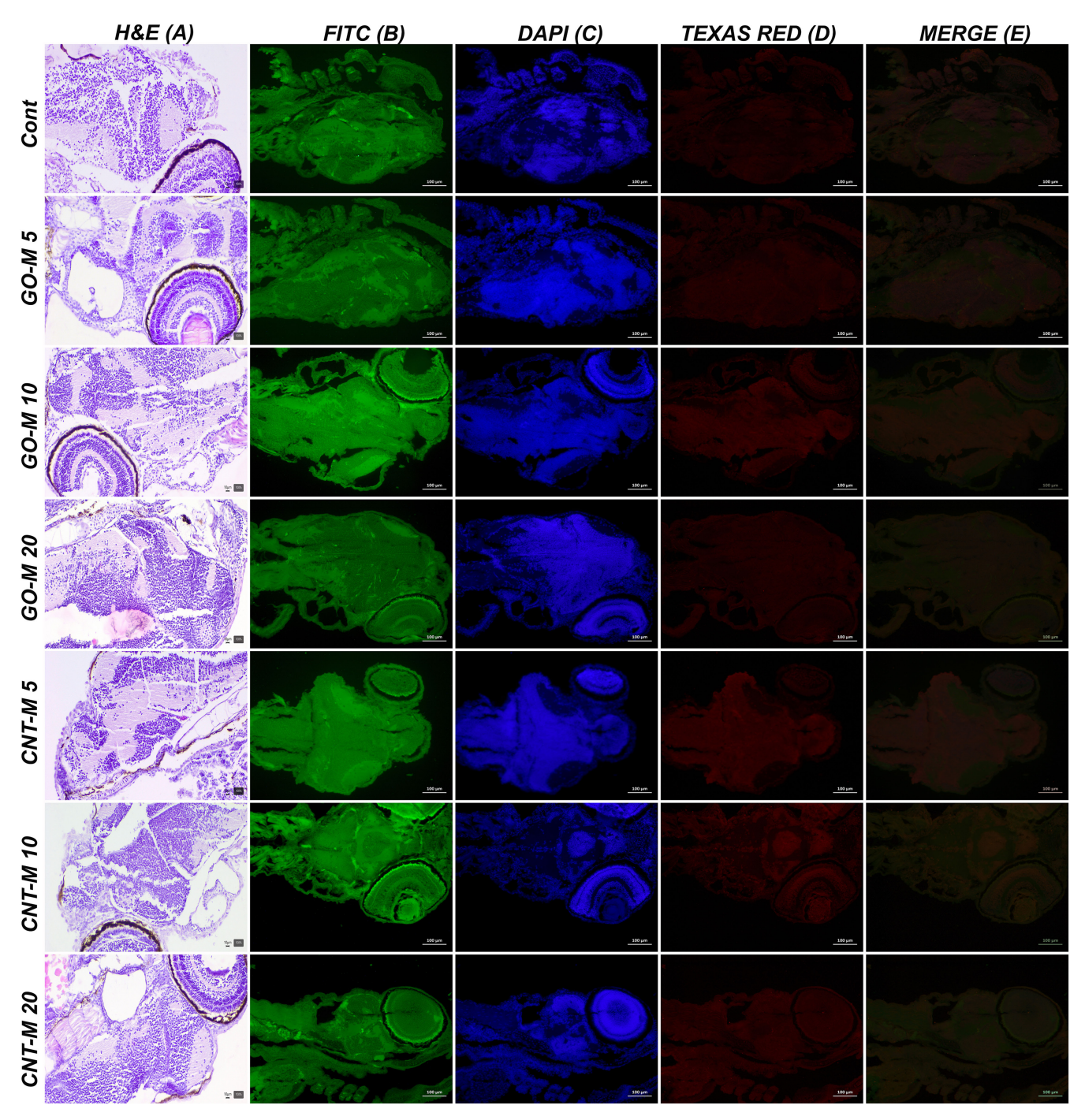


FIGURE 14 | Representative images of zebrafish brain tissue illustrating histopathological alterations and immunofluorescent markers of oxidative and nucleolar stress following exposure to various concentrations of GO-M and CNT-M nanomaterials. (A) H&E staining reveals tissue degeneration and necrosis. (B) Immunofluorescence staining for 8-OHdG (FITC channel) indicating oxidative DNA damage. (C) Nuclear counterstaining with DAPI. (D) NOP10 expression visualized using TEXAS RED, indicating nucleolar stress. (E) Merged images showing co-localization of markers. Scale bars: $10\,\mu$ m for H&E images; $100\,\mu$ m for immunofluorescence images.

pathological alterations. Similarly, exposure to low concentrations of both GO-M and CNT-M (5 mg/L) did not result in any observable tissue damage, indicating a lack of neurotoxic effects at these levels. At a concentration of 10 mg/L, GO-M exposure led to very mild vascular hyperemia, although this change was not statistically significant. A higher dose of GO-M (20 mg/L) induced mild signs of degeneration within the brain tissue. In contrast, exposure to CNT-M at 10 mg/L resulted in comparable levels of mild hyperemia, again without statistically significant difference. However, at the highest tested concentration of CNT-M (20 mg/L), more pronounced neurotoxic effects were observed, including moderate levels of brain tissue degeneration and evidence of mild necrosis. These findings suggest a dosedependent pattern of neurotoxicity, particularly in the CNT-M-exposed groups, where pathological changes became more evident with increasing concentration.

Histopathological alterations are considered reliable indicators of tissue-level damage caused by toxic substances. In this context, the absence of structural disruption at lower concentrations of GO-M and CNT-M suggests minimal neurotoxicity, while the

more substantial damage observed at higher concentrations, especially with CNT-M, underscores its greater neurotoxic potential. These observations also align with previous reports indicating that melamine may induce organ-specific pathological changes, primarily affecting the kidneys more severely than other tissues (Yang et al. 2022).

To further investigate potential neurotoxic mechanisms, oxidative DNA damage and nucleolar stress were assessed in zebrafish brain tissue using immunofluorescence staining for 8-OHdG and NOP10, respectively (Figure 14). In control specimens, as well as in those exposed to 5 and 10 mg/L of GO-M, expression levels of both markers remained negative. Mild cytoplasmic expression of 8-OHdG and NOP10 was detected in neuropils following exposure to 20 mg/L GO-M, suggesting the initiation of oxidative and nucleolar stress at this higher concentration. CNT-M exposure led to a more pronounced response. While 5 mg/L CNT-M did not alter expression levels, exposure to 10 mg/L resulted in mild cytoplasmic positivity for both 8-OHdG and NOP10. At 20 mg/L, a moderate increase in expression was evident in neuropil regions, indicating progressive stress accumulation. These

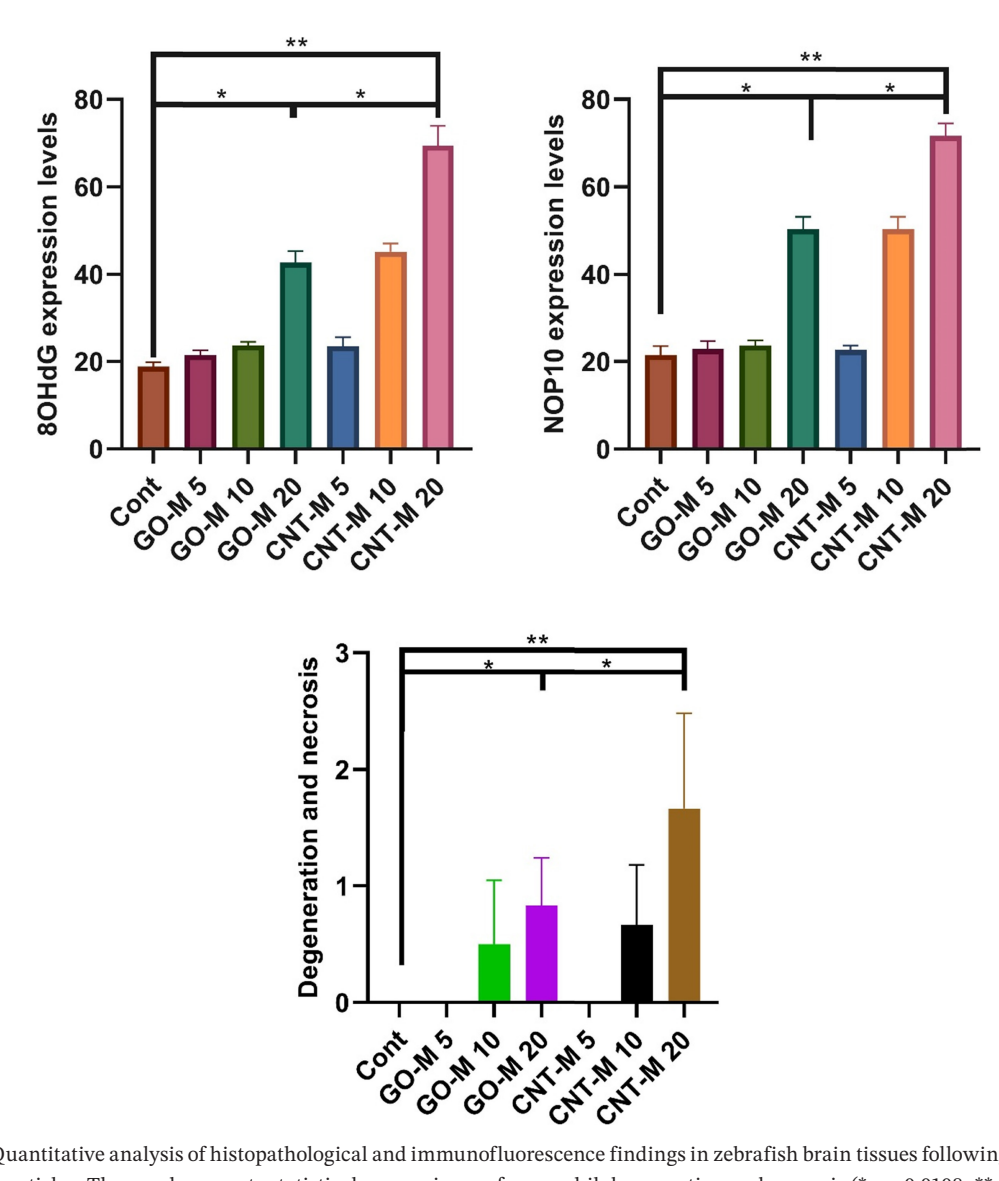


FIGURE 15 | Quantitative analysis of histopathological and immunofluorescence findings in zebrafish brain tissues following exposure to GO-M and CNT-M nanoparticles. The graph presents statistical comparisons of neurophil degeneration and necrosis (* p = 0.0108, ** p = 0.0022), 8-0HdG expression levels (* p = 0.0108, ** p = 0.0028) and NOP10 expression levels (* p = 0.0108, ** p = 0.0022).

molecular markers clearly demonstrate that both oxidative and nucleolar stress intensify with increasing nanoparticle concentration, with CNT-M inducing a stronger response than GO-M.

The immunofluorescence data support the hypothesis that melamine-functionalized carbon-based nanomaterials can cause neurotoxicity via oxidative and nucleolar stress pathways. The heightened sensitivity of neuronal cells, as indicated by increased expression of stress markers in neuropils, suggests that the central nervous system is particularly vulnerable to nanoparticle-induced damage. Overall, these results highlight CNT-M's greater potential to elicit neurotoxic effects compared to GO-M, especially at higher concentrations.

ROS, generated both endogenously through aerobic metabolism and exogenously by environmental agents such as chemical carcinogens and ionizing radiation, can inflict damage on genomic DNA. Among the most prevalent and mutagenic oxidative DNA lesions is 8-OHdG, a modified guanine base formed in response to ROS. 8-OHdG is highly mutagenic due to its ability to mispair with cytosine (C) or adenine (A) during DNA replication, resulting in G:C to T:A transversions both in vitro and in vivo. Consequently, 8-OHdG is widely recognized as a reliable biomarker for oxidative DNA damage (Ke et al. 2010). In our study, the levels of 8-OHdG in zebrafish brain tissue did not significantly increase in the low-concentration GO-M groups (5 and 10 mg/L), suggesting that these doses did not induce melamine-related oxidative DNA damage (Figure 15). This represents the first report investigating melamine's impact on oxidative DNA damage in a fish model. Interestingly, among all the tested conditions, only the CNT-M 20 mg/L group showed a notable elevation in 8-OHdG expression, indicating a dosedependent oxidative genotoxic effect for CNT-M, but not for GO-M (Figure 15).

Furthermore, marked differences in biomarker responses, particularly 8-OHdG and NOP10 expression, between GO-M 20 and CNT-M 20 groups highlight the influence of distinct physicochemical characteristics of the nanoparticles. Differences in surface area, shape, dispersibility, and protein corona formation may contribute to variations in cellular uptake and subcellular localization (Kopac 2021). The tubular morphology of CNT-M, for instance, may promote more efficient penetration of lipid membranes and interaction with nuclear DNA or nucleolar components, thereby exacerbating its toxic potential.

This hypothesis is supported by previous findings, where Wu et al. (2009) reported low melamine accumulation in brain tissue, and Chu et al. (2013) demonstrated short melamine half-lives. However, in our study, elevated NOP10 expression in the GO-M 20, CNT-M 10, and CNT-M 20 groups suggests that melamine-modified nanomaterials may induce nucleolar stress and potentially activate alternative programmed cell death pathways, possibly linked to DNA damage (Pereboom et al. 2011). Our data indicate that NOP10 holds promise as a biomarker for detecting neurotoxicity and nucleolar stress in zebrafish. While further studies are required to validate its specificity and sensitivity across different toxicity mechanisms, the present results support its use in zebrafish models as a valuable tool for mechanistic toxicology research.

4 | Conclusion

Growing concerns over melamine exposure, particularly through food contamination, highlight the urgent need to understand its toxicological effects, especially when integrated with nanomaterials. In this study, we systematically evaluated the physiological, morphological, histopathological, and immunohistochemical responses of zebrafish larvae following short-term exposure to GO-M and carbon nanotubes (CNT-M). Our results show that GO-M nanoparticles exhibit significantly lower toxicity than CNT-M, suggesting a comparatively safer profile for GO-based nanostructures modified with melamine. This research provides valuable insight into how nanomaterial shape, surface chemistry, and functionalization collectively influence biological responses. Despite being functionalized with the same organic molecule, the distinct structural and physicochemical properties of GO and CNT led to markedly different toxicological outcomes. These findings underscore the importance of considering nanocarbon architecture when evaluating potential environmental and biological risks.

By leveraging the zebrafish model, our work contributes to the growing body of evidence supporting its utility in environmental toxicology and human health risk assessment. Moreover, this study advances our understanding of melamine's interaction with engineered nanomaterials and the resulting implications for aquatic organisms. These findings may inform future regulatory strategies, promote safer nanomaterial design, and guide the monitoring of melamine-related hazards under environmentally relevant exposure scenarios.

Acknowledgements

This work was supported by the Izmir Institute of Technology Scientific Research Projects under the program of ADEP (Project no: 2024IYTE-2-0012).

Conflicts of Interest

The authors declare no conflicts of interest.

Data Availability Statement

The data that support the findings of this study are available from the corresponding author upon reasonable request.

References

Ahmed, Z. S. O., M. K. Galal, E. A. Drweesh, et al. 2021. "Protective Effect of Starch-Stabilized Selenium Nanoparticles Against Melamine-Induced Hepato-Renal Toxicity in Male Albino Rats." *International Journal of Biological Macromolecules* 191: 792–802.

Alak, G., A. Ucar, A. Ç. Yeltekin, S. Ç. Çomaklı, et al. 2018. "Neuroprotective Effects of Dietary Borax in the Brain Tissue of Rainbow Trout (Oncorhynchus Mykiss) Exposed to Copper-Induced Toxicity." *Fish Physiology and Biochemistry* 44, no. 5: 1409–1420. https://doi.org/10.1007/s10695-018-0530-0.

Alak, G., A. Ucar, A. Ç. Yeltekin, V. Parlak, et al. 2018. "Neurophysiological Responses in the Brain Tissues of Rainbow Trout (Oncorhynchus Mykiss) Treated with Bio-Pesticide." *Drug and Chemical Toxicology* 42, no. 2: 203–209. https://doi.org/10.1080/01480545.2018.1526180.

- Alak, G., A. Ç. Yeltekin, A. Uçar, V. Parlak, H. Türkez, and M. Atamanalp. 2019. "Borax Alleviates Copper-Induced Renal Injury via Inhibiting the DNA Damage and Apoptosis in Rainbow Trout." *Biological Trace Element Research* 191, no. 2: 495–501. https://doi.org/10.1007/s12011-018-1622-5.
- Alak, G., A. Ç. Yeltekin, F. B. Özgeriş, et al. 2019. "Therapeutic Effect of N-Acetyl Cysteine as an Antioxidant on Rainbow Trout's Brain in Cypermethrin Toxicity." *Chemosphere* 221: 30–36. https://doi.org/10.1016/j.chemosphere.2018.12.196.
- Alak, G., F. B. Özgeriş, A. Ç. Yeltekin, et al. 2020. "Hematological and Hepatic Effects of Ulexite in Zebrafish." *Environmental Toxicology and Pharmacology* 80: 103496. https://doi.org/10.1016/j.etap.2020.103496.
- Alak, G., S. Yıldırım, A. B. U. Kaplan, et al. 2025. "Evaluation of the Effects of Carbamazepine-Loaded Chitosan-Coated PLGA-Zein Nanoparticles on Pilocarpine-Induced Seizure Model in Zebrafish Larvae: Developmental Toxicity and Behavioral Assays." *Environmental Toxicology and Chemistry*: vgae086.
- Algethami, F. K., H. M. Marwani, N. Raza, A. M. Asiri, and M. M. Rahman. 2024. "Non-Enzymatic Electrochemical Detection of Melamine in Dairy Products by Using CuO Decorated Carbon Nanotubes Nanocomposites." *Food Chemistry* 445: 138792.
- Amudi, K., A. Yiğit, N. Menges, and P. T. Pınar. 2023. "Highly Selective Electrochemical Sensor for New Generation Targeted-Anticancer Drug Ibrutinib Using Newly Synthesized Nanomaterial GO-NH-B (OH) 2@ AgNPs Modified Glassy Carbon Electrode." *Measurement* 216: 112978.
- An, L., and W. Sun. 2017. "A Brief Review of Neurotoxicity Induced by Melamine." *Neurotoxicity Research* 32, no. 2: 301–309.
- An, L., Z. Li, and T. Zhang. 2013. "Reversible Effects of Vitamins C and E Combination on Oxidative Stress-Induced Apoptosis in Melamine-Treated PC12 Cells." *Free Radical Research* 48, no. 2: 239–250. https://doi.org/10.3109/10715762.2013.861598.
- Atamanalp, M., V. Parlak, F. B. Özgeriş, et al. 2021. "Treatment of Oxidative Stress, Apoptosis, and DNA Injury with N-Acetylcysteine at Simulative Pesticide Toxicity in Fish." *Toxicology Mechanisms and Methods* 31, no. 3: 224–234. https://doi.org/10.1080/15376516.2021. 1871794.
- Banerjee, S., and S. S. Wong. 2002. "Functionalization of Carbon Nanotubes With a Metal-Containing Molecular Complex." *Nano Letters* 2, no. 1: 49–53.
- Bangeppagari, M., S. H. Park, R. R. Kundapur, and S. J. Lee. 2019. "Graphene Oxide Induces Cardiovascular Defects in Developing Zebrafish (Danio Rerio) Embryo Model: In-Vivo Toxicity Assessment." *Science of the Total Environment* 673: 810–820.
- Bashir, D. W., M. M. Rashad, Y. H. Ahmed, et al. 2021. "The Ameliorative Effect of Nanoselenium on Histopathological and Biochemical Alterations Induced by Melamine Toxicity on the Brain of Adult Male Albino Rats." *Neurotoxicology* 86: 37–51.
- Bashir, N., T. Ali, I. Khan, A. Habib, N. Iqbal, and A. Afzal. 2025. "Ultrasensitive Carbon Nitride Nanosheets for Multiplex Sensing of Rhodamine B and Methylene Blue." *Diamond and Related Materials* 153: 112073.
- Benedetto, A., S. Squadrone, M. Prearo, et al. 2011. "Evaluation of ABC Efflux Transporters Genes Expression in Kidney of Rainbow Trout (Oncorhynchus Mykiss) Fed with Melamine and Cyanuric Acid Diets." *Chemosphere* 84, no. 5: 727–730.
- Bondy, S. C., and A. Campbell. 2005. "Developmental Neurotoxicology." *Journal of Neuroscience Research* 81, no. 5: 605–612.
- Borah, A. R., M. Gogoi, R. Goswami, A. Borah, and S. Hazarika. 2024. "Integrating Amine Functionalized Chiral Graphene Oxide Nanosheet Onto Cellulose Acetate Electrospun Nanofiber Membrane for Enantioselective Separation of Ibuprofen." *Journal of Membrane Science* 693: 122329.

- Bridi, D., S. Altenhofen, J. B. Gonzalez, G. K. Reolon, and C. D. Bonan. 2017. "Glyphosate and Roundup Alter Morphology and Behavior in Zebrafish." *Toxicology* 392: 32–39.
- Bulut, A., M. Yurderi, İ. E. Ertas, M. Celebi, M. Kaya, and M. Zahmakiran. 2016. "Carbon Dispersed Copper-Cobalt Alloy Nanoparticles: A Cost-Effective Heterogeneous Catalyst With Exceptional Performance in the Hydrolytic Dehydrogenation of Ammonia-Borane." *Applied Catalysis B: Environmental* 180: 121–129.
- Celebi, M., and E. G. Söğüt. 2022. "High-Efficiency Removal of Cationic Dye and Heavy Metal Ions From Aqueous Solution Using Amino-Functionalized Graphene Oxide, Adsorption Isotherms, Kinetics Studies, and Mechanism." *Turkish Journal of Chemistry* 46, no. 5: 1577–1593.
- Chen, H. C., W. W. Feng, G. Audira, et al. 2024. "Evaluation of Sub-Chronic Toxicity of Melamine via Systematic or Oral Delivery in Adult Zebrafish Based on Behavioral Endpoints." *Neurotoxicology* 102: 68–80.
- Chen, X., X. I. N. Hai, and J. Wang. 2016. "Graphene/Graphene Oxide and Their Derivatives in the Separation/Isolation and Preconcentration of Protein Species: A Review." *Analytica Chimica Acta* 922: 1–10.
- Chen, Y., Y. Li, D. Sun, D. Tian, J. Zhang, and J. J. Zhu. 2011. "Fabrication of Gold Nanoparticles on Bilayer Graphene for Glucose Electrochemical Biosensing." *Journal of Materials Chemistry* 21, no. 21: 7604–7611.
- Chen, Z., C. Yu, I. A. Khan, Y. Tang, S. Liu, and M. Yang. 2020. "Toxic Effects of Different-Sized Graphene Oxide Particles on Zebrafish Embryonic Development." *Ecotoxicology and Environmental Safety* 197: 110608.
- Chu, C. Y., K. O. Chu, C. S. Ho, et al. 2013. "Melamine in Prenatal and Postnatal Organs in Rats." *Reproductive Toxicology* 35: 40–47.
- Cunha, V., P. Rodrigues, M. M. Santos, P. Moradas-Ferreira, and M. Ferreira. 2018. "Fluoxetine Modulates the Transcription of Genes Involved in Serotonin, Dopamine and Adrenergic Signalling in Zebrafish Embryos." *Chemosphere* 191: 954–961.
- Day, D. B., M. M. Melough, J. T. Flynn, et al. 2024. "Environmental Exposure to Melamine and Its Derivatives and Kidney Outcomes in Children." *Environmental Research* 252: 118789. https://doi.org/10.1016/j.envres.2024.118789.
- Deng, J. H., L. Cheng, F. J. Wang, et al. 2015. "Ultralow Field Emission From Thinned, Open-Ended, and Defected Carbon Nanotubes by Using Microwave Hydrogen Plasma Processing." *Applied Surface Science* 324: 293–299.
- Dou, J., W. Hu, X. Zhang, and K. Jiang. 2024. "NOP10 Predicts Poor Prognosis and Promotes Pancreatic Cancer Progression." *BMC Cancer* 24, no. 1: 1394.
- Fan, R., J. Chen, X. Gao, and Q. Zhang. 2021. "Neurodevelopmental Toxicity of Alumina Nanoparticles to Zebrafish Larvae: Toxic Effects of Particle Sizes and Ions." *Food and Chemical Toxicology* 157: 112587.
- Feng, X., J. Wang, C. Zhang, Z. Du, H. Li, and W. Zou. 2018. "Fabrication and Characterization of Antistatic Epoxy Composite With Multi-Walled Carbon Nanotube-Functionalized Melamine Foam." *RSC Advances* 8, no. 27: 14740–14746.
- Ghulam, A. N., O. A. Dos Santos, L. Hazeem, B. Pizzorno Backx, M. Bououdina, and S. Bellucci. 2022. "Graphene Oxide (GO) Materials—Applications and Toxicity on Living Organisms and Environment." *Journal of Functional Biomaterials* 13, no. 2: 77.
- Gupta, N., S. M. Gupta, and S. K. Sharma. 2019. "Carbon Nanotubes: Synthesis, Properties and Engineering Applications." *Carbon Letters* 29, no. 5: 419–447.
- Huang, S. 2023. "Efficient Analysis of Toxicity and Mechanisms of Environmental Pollutants with Network Toxicology and Molecular Docking Strategy: Acetyl Tributyl Citrate as an Example." *Science of the*

Total Environment 905: 167904. https://doi.org/10.1016/j.scitotenv.2023. 167904.

Irani, M., A. T. Jacobson, K. A. Gasem, and M. Fan. 2017. "Modified Carbon Nanotubes/Tetraethylenepentamine for ${\rm CO_2}$ Capture." Fuel 206: 10–18.

Jebaranjitham, J. N., C. Mageshwari, R. Saravanan, and N. Mu. 2019. "Fabrication of Amine Functionalized Graphene Oxide–AgNPs Nanocomposite With Improved Dispersibility for Reduction of 4-Nitrophenol." *Composites Part B: Engineering* 171: 302–309.

Kahru, A., H. C. Dubourguier, I. Blinova, A. Ivask, and K. Kasemets. 2008. "Biotests and Biosensors for Ecotoxicology of Metal Oxide Nanoparticles: A Minireview." *Sensors* 8, no. 8: 5153–5170.

Karmakar, A., Q. Zhang, and Y. Zhang. 2014. "Neurotoxicity of Nanoscale Materials." *Journal of Food and Drug Analysis* 22, no. 1: 147–160.

Ke, Y., X. Duan, F. Wen, et al. 2010. "Association of Melamine Exposure With Urinary Stone and Oxidative DNA Damage in Infants." *Archives of Toxicology* 84: 301–307.

Keller, A. A., H. Wang, D. Zhou, et al. 2010. "Stability and Aggregation of Metal Oxide Nanoparticles in Natural Aqueous Matrices." *Environmental Science & Technology* 44, no. 6: 1962–1967.

Köktürk, M., S. Yildirim, A. Yiğit, et al. 2022. "What is the Eco-Toxicological Level and Effects of Graphene Oxide-Boramidic Acid (GO-ED-BA NP)?: In Vivo Study on Zebrafish Embryo/Larvae." *Journal of Environmental Chemical Engineering* 10, no. 5: 108443.

Köktürk, M., S. Yildirim, M. Atamanalp, et al. 2023. "Mitigation Potential of Zingerone and Rutin on Toxicity Mechanisms of Nickel to Zebrafish Based on Morphological, DNA Damage and Apoptosis Outcome Analysis." *Journal of Trace Elements in Medicine and Biology* 80: 127268.

Kopac, T. 2021. "Protein Corona, Understanding the Nanoparticle–Protein Interactions and Future Perspectives: A Critical Review." *International Journal of Biological Macromolecules* 169: 290–301.

Leon, V., A. M. Rodriguez, P. Prieto, M. Prato, and E. Vazquez. 2014. "Exfoliation of Graphite With Triazine Derivatives Under Ball-Milling Conditions: Preparation of Few-Layer Graphene via Selective Noncovalent Interactions." *ACS Nano* 8, no. 1: 563–571.

León, V., M. Quintana, M. A. Herrero, et al. 2011. "Few-Layer Graphenes From Ball-Milling of Graphite With Melamine." *Chemical Communications* 47, no. 39: 10936–10938.

Li, H., W. Song, S. Wang, et al. 2025. "Ingestion of Melamine Cleaning Sponges-Derived Microplastic Fibers Affects the Survival and Reproduction of Daphnia Magna." *Ecotoxicology and Environmental Safety* 290: 117814.

Liang, W., X. Chen, Y. Sa, Y. Feng, Y. Wang, and W. Lin. 2012. "Graphene Oxide as a Substrate for Raman Enhancement." *Applied Physics A* 109: 81–85.

Lütjens, L. H., S. Pawlowski, M. Silvani, U. Blumenstein, and I. Richter. 2023. "Melamine in the Environment: A Critical Review of Available Information." *Environmental Sciences Europe* 35, no. 1: 2. https://doi.org/10.1186/s12302-022-00707-y.

Manzoor, Q., M. A. Farrukh, M. T. Qamar, et al. 2024. "Polymer-Assisted Synthesis of Ternary Magnetic Graphene Oxide Nanocomposite for the Adsorptive Removal of Cr (VI) and Pb (II) Ions." *Heliyon* 10, no. 15: e35204.

Mao, Y., W. Xia, Y. Peng, and G. Xie. 2020. "Relationship Model Between Pore Wetting and Floatability of Active Carbon: Potential Guidance on Porous Mineral Flotation." *Minerals Engineering* 157: 106556.

Mohammadi, E., M. Zeinali, M. Mohammadi-Sardoo, M. Iranpour, B. Behnam, and A. Mandegary. 2020. "The Effects of Functionalization

of Carbon Nanotubes on Toxicological Parameters in Mice." *Human & Experimental Toxicology* 39, no. 9: 1147–1167.

Molino, C., I. Lacchetti, W. Cristiano, K. di Domenico, M. Carere, and D. Angeletti. 2025. "Zebrafish Embryo Model as a Tool for Ecotoxicological Studies in Central Italy's Transitional Waters." *Environmental Management* 75, no. 6: 1602–1614. https://doi.org/10.1007/s00267-025-02178-2.

Pei, X., A. Tandon, A. Alldrick, L. Giorgi, W. Huang, and R. Yang. 2011. "The China Melamine Milk Scandal and Its Implications for Food Safety Regulation." *Food Policy* 36, no. 3: 412–420.

Peng, G., L. Xing, J. Barrio, M. Volokh, and M. Shalom. 2018. "A General Synthesis of Porous Carbon Nitride Films With Tunable Surface Area and Photophysical Properties." *Angewandte Chemie International Edition* 57, no. 5: 1186–1192.

Pereboom, T. C., L. J. Van Weele, A. Bondt, and A. W. MacInnes. 2011. "A Zebrafish Model of Dyskeratosis Congenita Reveals Hematopoietic Stem Cell Formation Failure Resulting From Ribosomal Protein-Mediated p53 Stabilization." *Blood* 118, no. 20: 5458–5465.

Rodrigues, P., V. Cunha, L. Oliva-Teles, M. Ferreira, and L. Guimarães. 2020. "Norfluoxetine and Venlafaxine in Zebrafish Larvae: Single and Combined Toxicity of Two Pharmaceutical Products Relevant for Risk Assessment." *Journal of Hazardous Materials* 400: 123171.

Salam, M. A., and R. Burk. 2017. "Synthesis and Characterization of Multi-Walled Carbon Nanotubes Modified With Octadecylamine and Polyethylene Glycol." *Arabian Journal of Chemistry* 10: S921–S927.

Sen, K., S. Ali, D. Singh, K. Singh, and N. Gupta. 2021. "Development of Metal Free Melamine Modified Graphene Oxide for Electrochemical Sensing of Epinephrine." *FlatChem* 30: 100288.

Sharma, H. S., S. F. Ali, Z. R. Tian, et al. 2009. "Chronic Treatment With Nanoparticles Exacerbate Hyperthermia Induced Blood-Brain Barrier Breakdown, Cognitive Dysfunction and Brain Pathology in the Rat. Neuroprotective Effects of Nanowired-Antioxidant Compound H-290/51." *Journal of Nanoscience and Nanotechnology* 9, no. 8: 5073–5090.

Shayesteh, H., M. S. Khosrowshahi, H. Mashhadimoslem, F. Maleki, Y. Rabbani, and H. B. M. Emrooz. 2023. "Durable Superhydrophobic/ Superoleophilic Melamine Foam Based on Biomass-Derived Porous Carbon and Multi-Walled Carbon Nanotube for Oil/Water Separation." *Scientific Reports* 13, no. 1: 4515.

SinghDeo, S., S. S. Naser, A. Nandi, et al. 2025. "Intrinsic Physiochemical Insights to Green Synthesized Ag-Decorated GO Nanosheet for Photoluminescence and In Vivo Cellular Biocompatibility With Embryonic Zebrafish." *Colloids and Surfaces B: Biointerfaces* 245: 114212.

Sun, S., X. Gou, S. Tao, et al. 2019. "Mesoporous Graphitic Carbon Nitride (gC₃N₄) Nanosheets Synthesized From Carbonated Beverage-Reformed Commercial Melamine for Enhanced Photocatalytic Hydrogen Evolution." *Materials Chemistry Frontiers* 3, no. 4: 597–605.

Taşci, N., S. Çubuk, E. K. Yetimoğlu, and M. V. Kahraman. 2022. "A Novel Polymeric Fluorescence Sensor Based on Acrylated Citric Acid for Detection of Melamine Adulteration: Application in Milk Powder." *Food Chemistry* 394: 133525. https://doi.org/10.1016/j.foodchem.2022. 133525.

Uçar, A., V. Parlak, F. B. Özgeriş, A. Ç. Yeltekin, G. Alak, and M. Atamanalp. 2020. "Determination of Fipronil Toxicity by Different Biomarkers in Gill and Liver Tissue of Rainbow Trout (Oncorhynchus Mykiss)." *In Vitro Cellular & Developmental Biology - Animal* 56, no. 7: 543–549. https://doi.org/10.1007/s11626-020-00480-3.

Veisi, H., P. Safarimehr, and S. Hemmati. 2019. "Buchwald–Hartwig C–N Cross Coupling Reactions Catalyzed by Palladium Nanoparticles Immobilized on Thio Modified-Multi Walled Carbon Nanotubes as Heterogeneous and Recyclable Nanocatalyst." *Materials Science & Engineering, C: Materials for Biological Applications* 96: 310–318.

- Wang, H., N. Gao, W. Li, Z. Yang, and T. Zhang. 2015. "Melamine Induces Autophagy in Mesangial Cells via Enhancing ROS Level." *Toxicology Mechanisms and Methods* 25, no. 7: 581–587.
- Wang, H., J. Liu, S. Qiang, Y. Che, and T. Hu. 2024. "4-tert-Butylphenol Impairs the Liver by Inducing Excess Liver Lipid Accumulation via Disrupting the Lipid Metabolism Pathway in Zebrafish." *Environmental Pollution* 356: 124385.
- Wang, Z., Y. Fan, Y. Zhang, H. Liu, P. Liu, and Q. Wan. 2025. "Innovated Application of Melamine for High-Purity V2O5 Preparation." *Separation and Purification Technology* 359: 130534.
- Westerfield, M. 2000. The Zebrafish Book: A Guide for the Laboratory Use of Zebrafish Danio (Brachydanio) Rerio. 4th ed. ZFIN.
- Wu, Y. T., C. M. Huang, C. C. Lin, et al. 2009. "Determination of Melamine in Rat Plasma, Liver, Kidney, Spleen, Bladder and Brain by Liquid Chromatography–Tandem Mass Spectrometry." *Journal of Chromatography A* 1216, no. 44: 7595–7601.
- Yahyazadeh, A., S. Nanda, and A. K. Dalai. 2024. "Carbon Nanotubes: A Review of Synthesis Methods and Applications." *Reactions* 5, no. 3: 429–451.
- Yang, W., C. Liang, X. Zhang, et al. 2022. "Melamine Induced Changes in Histopathology of the Main Organs and Transcriptional Levels of MAPK Signaling Genes in Kidneys of Female Mice." *Environmental Toxicology* 37, no. 3: 585–592.
- Yiğit, A., M. Köktürk, S. Yıldırım, et al. 2024. "Effect of Boramidic Acid Modified Carbon Nanotubes on Neurological, Morphological and Physiological Responses of Zebrafish (*Danio rerio*) Embryos and Larvae." *Science of the Total Environment* 947: 174614.
- Yıldırım, S., M. Köktürk, A. Yığıt, et al. 2025. "Tuning Toxicity Profiles of Graphene Oxide Through Imidazole-Oxime Modification: Zebrafish as a Model System." *Environmental Toxicology and Chemistry* 44, no. 6: 1583–1595.
- Yuan, B., H. Sheng, X. Mu, et al. 2015. "Enhanced Flame Retardancy of Polypropylene by Melamine-Modified Graphene Oxide." *Journal of Materials Science* 50: 5389–5401.
- Zhang, H., Z. Zhang, Y. Hu, X. Yang, and S. Yao. 2011. "Synthesis of a Novel Composite Imprinted Material Based on Multiwalled Carbon Nanotubes as a Selective Melamine Absorbent." *Journal of Agricultural and Food Chemistry* 59, no. 4: 1063–1071.
- Zhao, Z., Q. Meng, T. Z. Sun, and B. Zhu. 2024. "Mannose Modified Targeted Immersion Vaccine Delivery System Improves Protective Immunity Against Infectious Spleen and Kidney Necrosis Virus in Mandarin Fish (Siniperca Chuatsi)." *Vaccine* 42, no. 11: 2886–2894.
- Zhu, Z. Z., Z. Wang, and H. L. Li. 2008. "Functional Multi-Walled Carbon Nanotube/Polyaniline Composite Films as Supports of Platinum for Formic Acid Electrooxidation." *Applied Surface Science* 254, no. 10: 2934–2940.